ACS SyntheticBiology

pubs.acs.org/synthbio

Research Article

Light-Induced Patterning of Electroactive Bacterial Biofilms

Fengjie Zhao,[#] Marko S. Chavez,[#] Kyle L. Naughton, Christina M. Niman, Joshua T. Atkinson, Jeffrey A. Gralnick, Mohamed Y. El-Naggar, and James Q. Boedicker*

Cite This: https://doi.org/10.1021/acssynbio.2c00024

Read Online

ACCESS | Metrics & More | Article Recommendations | Supporting Information

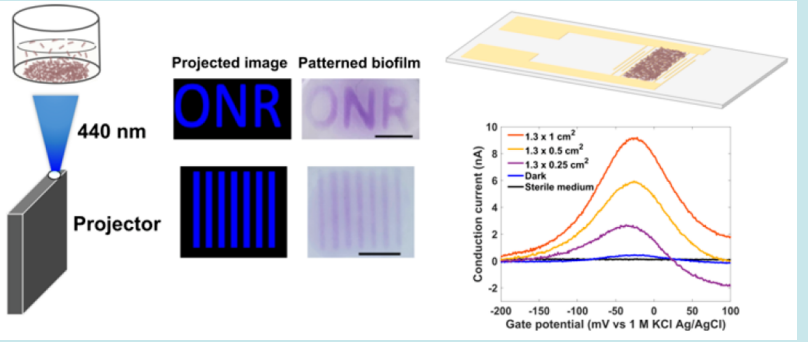

ABSTRACT: Electroactive bacterial biofilms can function as living biomaterials that merge the functionality of living cells with electronic components. However, the development of such advanced living electronics has been challenged by the inability to control the geometry of electroactive biofilms relative to solid-state electrodes. Here, we developed a lithographic strategy to pattern conductive biofilms of *Shewanella oneidensis* by controlling aggregation protein CdrAB expression with a blue light-induced genetic circuit. This controlled deposition enabled *S. oneidensis* biofilm patterning on transparent electrode surfaces, and electrochemical measurements allowed us to both demonstrate tunable conduction dependent on pattern size and quantify the intrinsic conductivity of the living biofilms. The intrinsic biofilm conductivity measurements enabled us to experimentally confirm predictions based on simulations of a recently proposed collision-exchange electron transport mechanism. Overall, we developed a facile technique for controlling electroactive biofilm formation on electrodes, with implications for both studying and harnessing bioelectronics.

KEYWORDS: *Shewanella oneidensis MR-1, biofilm patterning, extracellular electron transfer, electrochemical gating*

INTRODUCTION

Exoelectrogens can use extracellular electron transfer (EET) pathways to gain energy by respiring solid surfaces such as minerals and electrodes in anoxic environments.[1,2] *Shewanella oneidensis* MR-1 is one of the most studied model exoelectrogenic organisms, whose EET pathway includes a network of multiheme *c*-type cytochromes to route electrons from the cellular interior to external surfaces.[3−9] Electrons are transferred to external, solid electron acceptors indirectly via soluble flavins that serve as electron shuttles and directly via contact with the cell surface cytochromes, flavin-cytochrome complexes, or along membrane extensions that are proposed to act as nanowires.[10−13]

When performing direct electron transfer, exoelectrogens are able to colonize electrode surfaces and form living conductive biofilms, which allow for long-distance electron transport across neighboring cells on the micrometer-scale.[14] Electrochemical techniques have proved valuable for investigating the electron transport mechanisms in these biofilms, demonstrating that redox gradient-driven electron hopping is the basis of biofilm conduction in both *Geobacter* and *Shewanella*.[15−17] Such electroactive biofilms, acting as living biomaterials, have found applications in microbial fuel cells, microbial electrosynthesis cells, nanoparticle templating, and bioremediation.[18,19] In addition to these sustainability applications, electroactive biofilms have recently been proposed to form the basis of living electronics, hybrid devices that integrate cells on electrodes to combine the functionality of a biological system (e.g., for biosensing, biocomputing, or data storage) with the readout, stimulation, and amplification advantages of electronic circuitry.[14,20,21] To realize such hybrid technologies, it is important to develop new tools for controlling electroactive biofilm formation in relation to solid-state electrodes with high spatial resolution.

Synthetic biology strategies have recently been developed for regulating the EET capabilities of *S. oneidensis*, such as tuning

Received: January 16, 2022

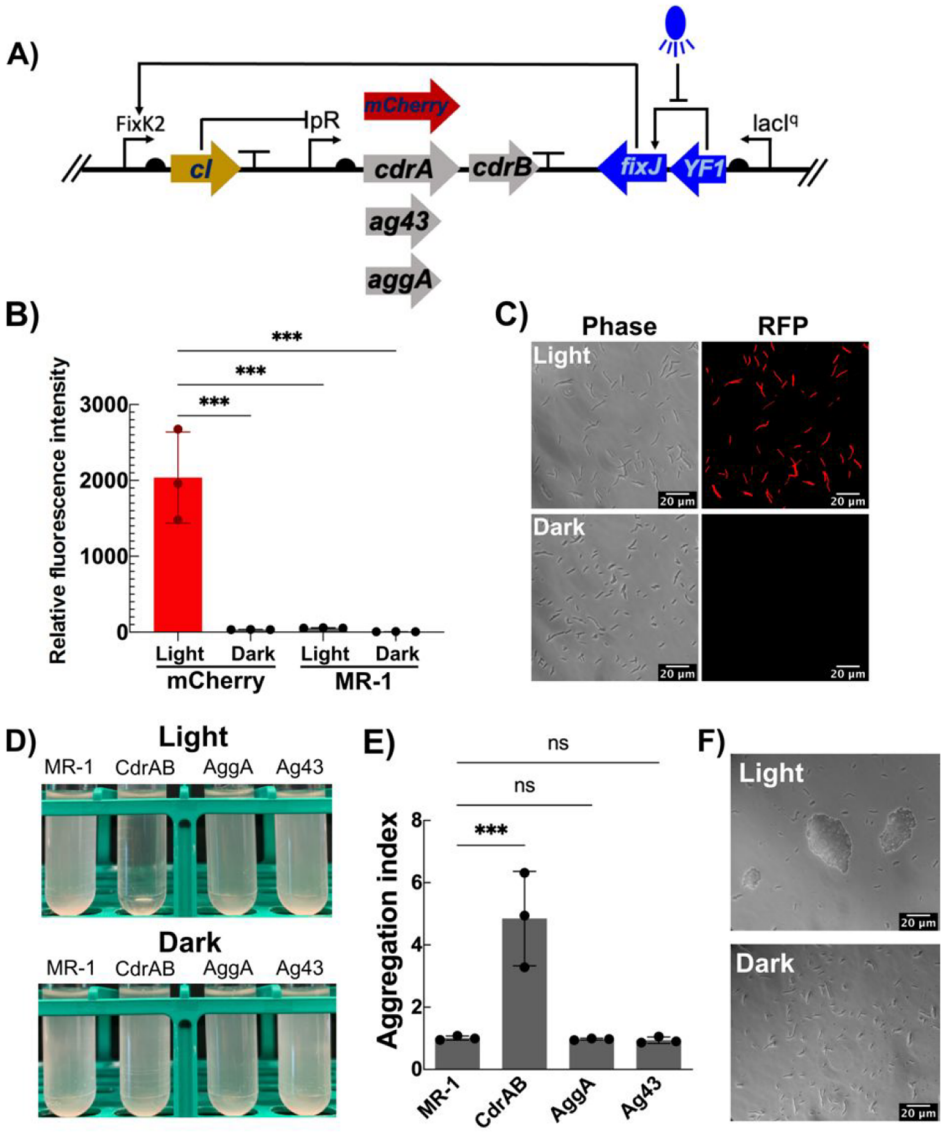

Figure 1. Characterization of the pDawn genetic circuit in *Shewanella* and selection of adhesive proteins for clumping *Shewanella* cells under blue light illumination. (A) The genetic circuit pDawn was used for light-induced expression of mCherry or different adhesive proteins. (B) Fluorescence intensity measurements of mCherry and wild type strains cultured under blue light and dark conditions, respectively. n = 3 independent biological experiments per group. p = 0.0001 for mCherry Light vs mCherry Dark, mCherry Light vs MR-1 Light, and mCherry Light vs MR-1 Dark (one-way ANOVA with Dunnett's multiple comparisons test). (C) Microscope observation for mCherry cells grown under blue light and dark conditions, respectively. (D) Cell clumping assay of *Shewanella* strains with different aggregation proteins expressed under blue light. (E) Aggregation indexes of different *Shewanella* strains. n = 3 independent biological experiments per group. p = 0.0007 for MR-1 vs CdrAB, p > 0.9999 for MR-1 vs AggA and MR-1 vs Ag43 (one-way ANOVA with Dunnett's multiple comparisons test). (F) Microscope observation for cell clusters of the CdrAB strain cultured under blue light and dark conditions, respectively. Data are shown as mean ± SD. Significance is indicated as ***p < 0.001 and ns (not significant) p > 0.05.

mtrCAB expression level with a native inducible system[22] and using clustered regularly interspaced short palindromic repeats interference (CRISPRi) to regulate the transcription of *mtrA*.[23] In a recent study, a quorum sensing-based population-state decision (PSD) system was constructed to link the EET network to population density.[24] The EET pathway has also been reconstructed successfully in *Escherichia coli* through heterologous expression of the MtrCAB complex.[25] The EET ability of engineered *E. coli* can be further enhanced through coexpression of CymA, adding exogenous flavins or modifying the cytochrome *c* maturation pathway.[26,27] Although much progress has been made in manipulating the EET machinery of *Shewanella*, very little work has been done in tuning EET through the controlled formation of conductive biofilms on solid-state electrodes. Many downstream applications and fundamental experimental measurements would benefit from the ability to precisely pattern electroactive biofilms on electrode surfaces.

In recent years, optogenetic approaches have been developed for spatial control of gene expression in bacteria as a response to illumination with light.[28−30] These techniques provide possible strategies to dynamically control cell−cell adhesions for patterning bacterial biofilms with high spatial and temporal precision. Some studies have utilized light-induced genetic circuits to control the expression of aggregation proteins that mediate cell−cell adhesion and realize bacterial

https://doi.org/10.1021/acssynbio.2c00024
ACS Synth. Biol. XXXX, XXX, XXX−XXX

biofilm patterning. A technique called "Biofilm Lithography" was recently developed, which used the blue light-induced pDawn genetic circuit to control the expression of *E. coli* cell-surface adhesin Ag43 in order to pattern *E. coli* biofilms with high spatial resolution.[31] Biofilm patterning of *E. coli* on various types of material surfaces has also been achieved by controlling biosynthesis of curli fibers in response to illumination with various wavelengths of light.[32] Optogenetic tools can also directly control protein activities to adjust bacterial biofilm formation, such as activating proteins involved in cyclic dimeric guanosine monophosphate (*c*-di-GMP) synthesis or hydrolysis[33] and toggling cell−cell adhesion through photoswitchable protein heterodimers.[34] Although the ability to pattern *E. coli* biofilms exists, electrochemical measurements of engineered, EET capable *E. coli* have yielded low electrical current[25] and had limitations for further applications compared with naturally electroactive bacteria. Similarly, biofilm patterning techniques have not previously been adapted for naturally electroactive bacteria. Inspired by these robust optogenetic patterning techniques, we set out to implement a similar strategy in the EET model organism *S. oneidensis* to enable light-patterning of naturally electroactive biofilms. Thus, biofilm size-dependent tunability of electron transport in conductive biofilms and the accurate determination of biofilm conductivity from the defined patterns can be possible.

In this work, we introduced the blue light-induced pDawn genetic circuit into *S. oneidensis* to control the expression of aggregation proteins CdrAB. CdrAB is a set of proteins found in *Pseudomonas aeruginosa* that helps to regulate adhesion and biofilm formation.[35,36] Biofilm patterning of the resulting CdrAB strain was first achieved on both plastic and glass substrates under blue light illumination. Next, we confirmed that it was possible to pattern the CdrAB strain onto transparent, indium tin oxide (ITO) electrode surfaces and that these patterned biofilms remained electrochemically active. By patterning biofilms on ITO interdigitated array (IDA) microelectrodes and performing electrochemical gating measurements, we demonstrated that biofilm conduction could be tuned by controlling the biofilm dimensions and determined the intrinsic redox conductivity of the patterned biofilms. To our knowledge, this is the first demonstration of light-based lithography of naturally electroactive biofilms on electrodes.

RESULTS

The pDawn Genetic Circuit Enables Blue Light-Induced Protein Expression in *S. oneidensis*. The light responsive pDawn genetic circuit has been used to control gene expression in *E. coli* and *P. aeruginosa*,[29,37] but has yet to be tested in *S. oneidensis*. To verify whether the blue light-induced pDawn genetic circuit is functional in *S. oneidensis*, we expressed the red fluorescent protein mCherry with the pDawn plasmid (Figure 1A) by irradiating the cells with blue light LEDs while culturing them in a shaking incubator. The relative fluorescence intensity of the mCherry strain was increased 58-fold under blue light illumination compared with that of those cells cultured in the dark (Figure 1B). The mCherry strain grown in the dark and the untransformed wild type cells grown either in the dark or under blue light illumination exhibited weak fluorescence intensity (Figure 1B). Bright red fluorescence could be seen in the fluorescence microscopy images of mCherry cells grown under blue light illumination, while fluorescence was not detected from microscopy for the cells grown in the dark (Figure 1C). Taken collectively, these results indicate that the pDawn light-activated transcriptional promoter can be used to optically regulate gene expression in *S. oneidensis*.

The Expression of CdrAB Can Mediate Cell−Cell Aggregation in *S. oneidensis*. One of the strategies for mediating bacterial cell−cell aggregation is to express outer membrane adhesive proteins involved in biofilm formation. Thus, several putative proteins that promote bacterial autoaggregation and biofilm formation from different species were selected to be expressed in *S. oneidensis* under the control of the pDawn genetic circuit, including Ag43 from *E. coli*[38,39] and CdrAB from a *P. aeruginosa* PAO1 two-partner secretion system[35,36] (Figure 1A). The native AggA aggregation protein from *S. oneidensis*[40,41] was also overexpressed using the pDawn genetic circuit (Figure 1A). To monitor protein expression, we then isolated the outer membrane fractions from our engineered *S. oneidensis* cells after culturing them under blue light and ran an SDS-PAGE gel. The results showed that Ag43, AggA, and CdrB were expressed and present on the outer membrane. However, we were unable to observe CdrA in the outer membrane fraction (Figure S1A). CdrA is a very large adhesion protein (~220 kDa for the unprocessed CdrA) that is transported to the cell surface by CdrB.[35,36] CdrA may aggregate on the outer membrane and thus be difficult to see in the SDS-PAGE gel. In *P. aeruginosa*, CdrA can be released from the cell surface through cleavage by the protease LapG.[42] An SDS-PAGE gel of the supernatant fraction from the CdrAB culture showed a visible band of the processed CdrA protein indicating that *Shewanella* may have homologous proteases that can cleave CdrA[43] (Figure S1B). After expressing LapG from *P. aeruginosa* in the CdrAB strain, there was increased CdrA visible in the supernatant fraction (Figure S1B), which further confirmed that CdrA was expressed and presented on the outer membrane.

Cells that cluster when grown in liquid culture will sediment to the bottom of culture tubes if not shaken, reducing the turbidity of the culture at the top of the tube. As shown in Figure 1D, expression of CdrAB under blue light illumination triggered obvious cell−cell aggregation and sedimentation in *S. oneidensis*. However, we were not able to detect cell−cell aggregation when inducing the expression of Ag43 or the overexpression of AggA (Figure 1D). The extent to which cell adhesion increased upon light-induced expression of the potential aggregation genes was quantified using an "aggregation index". This aggregation index measures the reduction of the culture turbidity at the top of the culture tube after settling (see Methods). The aggregation index of 4.85, measured for the CdrAB strain, indicated significant cell−cell adhesion relative to the WT MR-1 strain (Figure 1E). However, the strains with inducible expression of Ag43 or AggA showed aggregation indexes near 1, indicating no increased sedimentation relative to the WT MR-1 strain (Figure 1E). Microscopy confirmed many large cell clusters were formed due to the cell−cell aggregation of the CdrAB strain grown under blue light illumination, while no large cell clusters were observed under the dark culturing condition (Figure 1F). These results indicate that the expression of CdrAB can be controlled by light and mediate cell−cell aggregation in *S. oneidensis*.

Biofilm Formation Can Be Enhanced and Patterned by Expressing CdrAB in *S. oneidensis* under Blue Light. Bacterial biofilm formation is closely coupled to cell

https://doi.org/10.1021/acssynbio.2c00024
ACS Synth. Biol. XXXX, XXX, XXX−XXX

aggregation.[34] To verify that the biofilm formation of the CdrAB strain can be significantly enhanced when grown under blue light illumination, we performed a biofilm formation assay. Cells were grown in 96-well plates and exposed to blue light from a portable LED projector (Figure 2A). Crystal violet staining was used to quantify biofilm formation.[44] The results showed that the CdrAB strain formed robust biofilms under blue light illumination, while weak biofilms were formed in the dark (Figure 2B). Wild-type cells failed to form robust biofilms regardless of dark or blue light illuminated growth conditions (Figure 2B). Next, we optimized biofilm formation by systematically testing the impact of illumination intensity and time. We found that the extent of CdrAB biofilm formation reached a maximum with 110 μW/cm^2 light intensity and then decreased for light intensities exceeding 120 μW/cm^2 when grown overnight for 16 h (Figure S2A). This may be due to higher levels of light intensity negatively impacting cellular growth, reducing biofilm formation despite higher expression of CdrAB. CdrAB biofilm formation peaked after about 16 h and then decreased with increasing incubation time when illuminated at 110 μW/cm^2 (Figure S2B), indicating that biofilm formation changes dynamically with time. For all experiments described below, we used a light intensity of 110 μW/cm^2 for 16 h to control biofilm formation unless stated otherwise.

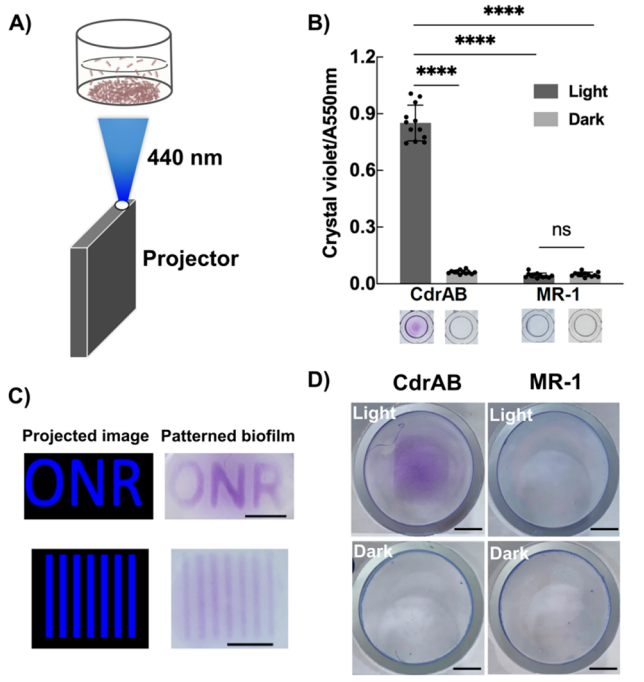

Figure 2. Light-induced biofilm formation and patterning. (A) Schematic for biofilm formation and patterning with blue light, performed with a portable LED projector. (B) Biofilm formation assay of CdrAB and wild type under blue light and dark conditions, respectively. $n = 12$ independent biological experiments per group. $p < 0.0001$ for CdrAB Light vs CdrAB Dark, CdrAB Light vs MR-1 Light and CdrAB Light vs MR-1 Dark (one-way ANOVA with Dunnett's multiple comparisons test). $p = 0.3466$ for MR-1 Light vs MR-1 Dark (two-tailed unpaired t test). (C) Biofilm patterning of CdrAB in 12-well plates. (D) Biofilm patterning of CdrAB on ITO coated glass coverslip. Scale bars, 0.5 cm. Data are shown as mean ± SD. Significance is indicated as ****$p < 0.0001$ and ns (not significant) $p > 0.05$.

Since CdrAB biofilm formation was significantly enhanced when grown under blue light illumination, we expected that the biofilm could also be patterned under blue light. We first cultured the cells in a 12-well polystyrene plate and illuminated various patterns on the bottom of the wells. Clear patterns ("ONR" and stripes, with a single strip width of 650 μm) were visible after staining with crystal violet, which is used to identify regions of biofilm formation (Figure 2C). We also optimized the illumination time (Figure S3A and S3B) and growth medium volume (Figure S3A and S3C) when patterning in the 12-well plates. Pattern formation was optimal when culturing in 1 mL defined minimal medium for 16 h, showing the sharpest contrast between exposed and unexposed regions of the plate, which was consistent with the results of biofilm formation assay described above (Figure S2B).

To test our patterning strategy on surfaces other than plastic, we moved to attempt biofilm patterning on glass surfaces by illuminating various patterns on the underside of glass bottom dishes. As shown in Figure S4, clear biofilm patterns were observed after crystal violet staining (Figure S4A). Microscopy revealed an increased and more uniform layer of cells in areas of the substrate exposed to blue light (Figure S4B). These results indicate the potential for patterning biofilms of *S. oneidensis* on a variety of substrates. For electrochemical measurements, biofilms would need to be patterned on electrodes. So next, we tested whether it was possible to pattern biofilms on transparent electrodes by culturing cells in a glass tube vertically adhered to the surface of a conductive, planar indium tin oxide (ITO) coated glass coverslip (Figure

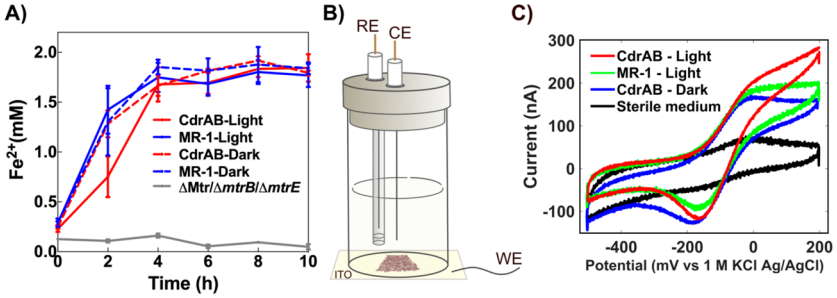

Figure 3. Extracellular electron transfer capability of CdrAB cells after being cultured under blue light and electrochemical activity for patterned CdrAB biofilms. (A) Ferrozine assay for CdrAB and wild type after being cultured under blue light and dark conditions, respectively. Data are shown as mean ± SD from 3 independent biological experiments. (B) Schematic of the bioreactor used for electrochemical measurements. (C) Representative cyclic voltammetry curves for CdrAB and wild type.

https://doi.org/10.1021/acssynbio.2c00024
ACS Synth. Biol. XXXX, XXX, XXX−XXX

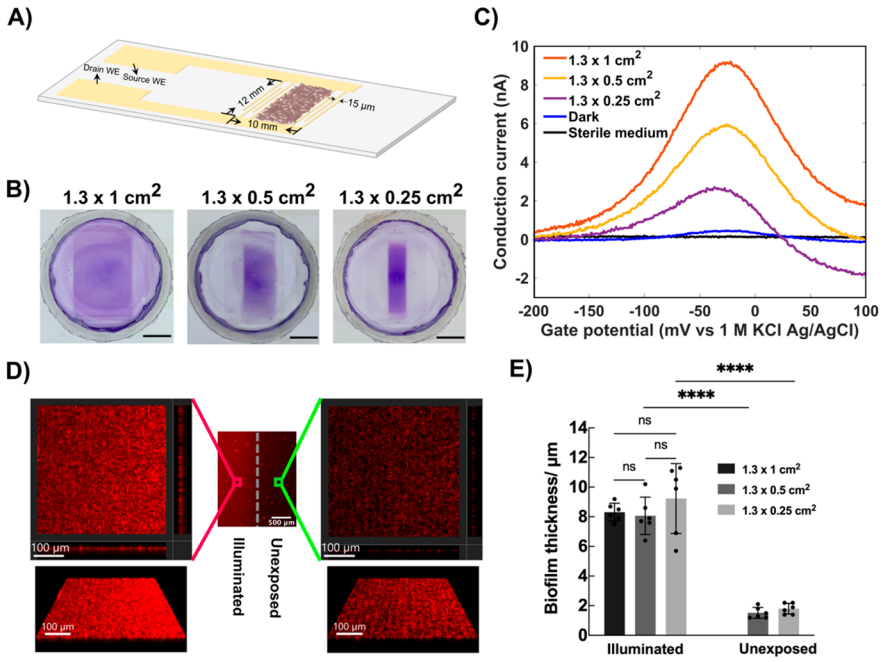

Figure 4. Electrochemical gating measurements for patterned CdrAB biofilms of different sizes. (A) Diagram of the custom transparent ITO IDA electrode. (B) Crystal violet staining of patterned biofilms with different sizes after the gating measurements, Scale bars, 0.5 cm. (C) Representative conduction currents curves of patterned biofilms with different sizes calculated from electrochemical gating measurements. (D) Confocal microscope images of biofilms on ITO IDA in blue-light illuminated region and unexposed region (1.3 × 0.25 cm^2 pattern sample). (E) Thicknesses of biofilms on ITO IDAs in the blue-light illuminated region and unexposed region of the patterned biofilm. $n = 6$ average biofilm thickness values calculated from 6 cross sections of three different confocal microscopy images per group. The method for biofilm thickness analysis is shown in Supplementary Methods and Figure S14. $p = 0.9587$ for illuminated 1.3 × 1 cm^2 vs 1.3 × 0.5 cm^2, $p = 0.5862$ for illuminated 1.3 × 0.1 cm^2 vs 1.3 × 0.25 cm^2 and $p = 0.4291$ for illuminated 1.3 × 0.5 cm^2 vs 1.3 × 0.25 cm^2 (one-way ANOVA with Dunnett's multiple comparisons test). $p < 0.0001$ for 1.3 × 0.5 cm^2 illuminated vs unexposed and 1.3 × 0.25 cm^2 illuminated vs unexposed (two-tailed unpaired t test). Data are shown as mean ± SD. Significance is indicated as ****$p < 0.0001$ and ns (not significant) $p > 0.05$.

S5A), a setup which can be used to make electrochemical measurements postpatterning. Since we observed that medium volume had an effect on biofilm patterning, we first optimized patterning in the glass tube setup by incubating different culture volumes in glass tubes adhered to cover glass with similar thickness to that of the ITO-coated coverslips. The patterned rectangular biofilms were most visible when 1 mL minimal medium was used to culture cells in the glass tube vessels (Figure S5B and S5C). Then, we added 1 mL minimal medium to the glass tubes adhered to ITO coverslips and cultured the cells on the ITO surface by illuminating it with a rectangular pattern. As expected, the results showed that CdrAB biofilms could be patterned on the ITO surface under blue light illumination (Figure 2D).

The Expression of CdrAB Does Not Significantly Hinder Extracellular Electron Transfer Activity. Expressing outer membrane proteins on the cell surface of *S. oneidensis* may reduce the quantity of outer membrane cytochromes, which in turn may hinder extracellular electron transfer (EET).[45] To verify whether the expression of CdrAB would hinder the EET capability of *S. oneidensis*, we performed a ferrozine assay to compare the Fe^{3+} reduction capabilities of CdrAB and wild type strains after being cultured under blue light illumination and dark conditions, respectively. We also tested a mutant strain, ΔMtr/Δ*mtrB*/Δ*mtrE*, which lacks genes encoding periplasmic and outer-membrane cytochromes critical for EET, as a negative control.[46] Our results showed that the Fe^{3+} reduction of blue light illuminated CdrAB cells was initially slightly slower than that of CdrAB cells grown in the dark and wild type cultured either under blue light or in the dark, but then after a few hours, the extent of reduction was similar (Figure 3A). This indicated that the expression of CdrAB on the outer membrane of *S. oneidensis* may have interfered with the expression level or functionality of outer membrane cytochromes. A TMBZ heme staining SDS-PAGE gel was performed to determine the concentration of outer membrane cytochromes, which confirmed that CdrAB had a lower quantity of outer membrane cytochromes after being cultured under blue light (Figure S6). Reduced expression of MtrCAB is likely the reason for the slower Fe^{3+} reduction rate for CdrAB cells after growth in blue light. These CdrAB cells eventually achieved a similar Fe^{3+} reduction level to that of the controls. Increased expression of MtrCAB in the absence of blue light illumination during the ferrozine experiments may have contributed to this faster iron reduction rate. Overall, after expressing CdrAB under blue light, the CdrAB strain maintained its EET capability and could achieve a considerable Fe^{3+} reduction level (Figure 3A).

Since CdrAB cells could maintain EET activity after expressing CdrAB, we reasoned that the patterned biofilms also remained electrochemically active, that is, able to exchange electrons with electrodes. To this end, CdrAB cells were incubated overnight in planar ITO-bottom glass tube reactors with a defined, rectangular light pattern projected onto the base of the reactors from below (Figure 2A and 2D and 3B). As non-pattern-forming controls, glass tube reactors containing wild type cells exposed to the same projected light pattern and CdrAB cells kept in the dark were also incubated overnight.

https://doi.org/10.1021/acssynbio.2c00024
ACS Synth. Biol. XXXX, XXX, XXX−XXX

After overnight patterning and washing, the ITO bottom reactors were transferred to an anaerobic chamber for electrochemical measurements. We performed cyclic voltammetry (CV) scans, which monitor redox activity of the CdrAB cells' outer membrane cytochromes.[47] We observed that the CdrAB strain, both under light and dark conditions, remained capable of electrode reduction at the same redox potential as the wild type (Figure 3C). We also observed that, under the above experimental conditions, light patterned CdrAB produced more current than the dark condition and the wild type, likely due to the enhanced biofilm formation (Figure 3C). To improve cytochrome expression, biofilm patterning was also attempted under anaerobic conditions. We observed that biofilm patterning was still viable under anaerobic conditions (Figure S7) and that the CdrAB strain was again capable of electrode reduction at the same redox potential as the wild type (Figure S8). However, we observed increased cell attachment in the unexposed regions after anaerobic patterning (Figure S7). Thus, to minimize nonpatterned cell attachment, all subsequent light-patterning was performed under aerobic conditions prior to anaerobic electrochemical measurements.

Electrochemical Activity and Conductance of Patterned Biofilms Are Proportional to Biofilm Surface Area. Controllable size-dependent conduction within electroactive biofilms may have significant implications for studying and harnessing microbes as conductive materials in bioelectronics. To assess if tuning biofilm size altered overall electron transport through the patterned biofilms, we investigated the electrochemical activity of patterned biofilms as a function of biofilm size. Custom ITO interdigitated array (IDA) electrodes were used to measure biofilm conductance. An IDA is a patterned electrode with two sets of conductive regions (electrode fingers) and an interspersed nonconductive region (gaps between electrode fingers) that enables the measurement of conduction current through materials bridging the electrodes. With the IDA geometry, one set of fingers acts as the source (S) electrodes while the other acts as the drain (D) electrodes (Figure 4A), enabling electron transport through the biofilm, from the source electrode to the drain electrode. Additionally, the IDA geometry enables a large number of $S-D$ electrode pair crossings for a biofilm patterned over it, enhancing conductance signal as compared to biofilm conductance measured using only two side-by-side electrodes.[17,48]

Three different sizes of biofilms were patterned onto custom ITO IDA-bottom glass tube reactors by projecting rectangular light patterns with the following dimensions: 1.3 × 0.25 cm^2 (small pattern), 1.3 × 0.5 cm^2 (medium pattern), and 1.3 × 1 cm^2 (large pattern), along with a nonpatterned dark condition. Crystal violet staining clearly showed that three different sizes of biofilms were patterned (Figure 4B). The lines' edge roughness of the 1.3 × 0.25 cm^2 pattern on our IDA were 37.5 and 51.3 μm for the left and right edges, respectively (Figure S9 and Supplementary Methods). And the width of single strip we had patterned on the 12-well plate was around 650 μm (Figure 2C). In prior work, the same genetic circuit was used to control the aggregation protein Ag43 expression for *E. coli* patterning, which could reach a feature size at the scale of 25 μm by using a film photomask.[31] Thus, this patterning tool enables sufficient control over conductive biofilm geometry for size-dependent conductance measurements.

Electrochemical gating was used to measure biofilm conduction current for the four different conditions. A fixed potential offset was maintained between the source and drain working electrodes (WEs) of a custom ITO IDA to serve as a driving force for conduction[17] and the conduction current of patterned biofilms bridging the WEs (Figure 4A) was measured as the potentials were swept at each WE. From the raw IDA source and drain CVs of our gating measurements, we observed increasing electrochemical activity as a function of increasing patterned biofilm size, with the dark condition producing the least amount of current (Figure S10). By plotting the conduction current (I_{cond}) vs the gate potential (E_G, average potential of WEs during the gating scan), our results showed peak-shaped curves centered at the redox potential of *Shewanella* EET proteins (Figure 4C), as expected for a redox conduction mechanism,[17] indicating cell-to-cell long-distance electron transport within light patterned biofilms. From our size-dependent I_{cond} vs E_G data, we observed increasing conduction current as a function of increasing biofilm size (Figure 4C), as expected since cells form the conduction channel between the source and drain electrodes. In other words, as we increase the biofilm size to cover more gaps between source and drain electrodes, we see increased conduction through the biofilm since we are increasing the length of the conductive channel that current can flow through from the source to the drain electrode (Figure S11). An electrochemical gating measurement performed on the dark condition produced the lowest conduction current (Figure 4C), likely due to the inability of the nonpatterned biofilms to bridge the source and drain electrodes, as compared to the patterned biofilms (Figure S12 and Figure 4D). We observed a 30-fold increase in conduction current for the large patterned biofilms relative to the dark condition. Due to the large working area of our custom IDA and our ability to pattern continuous biofilms, we were able to detect 10-fold larger conduction currents than what was previously measured in *S. oneidensis*.[16]

In addition to the size dependent conduction current measurements, the same sized biofilms, along with a dark condition, were patterned onto planar ITO-bottom glass tube reactors ahead of CV measurements. These CVs gave results similar to those of our raw IDA source and drain CVs, showing increasing electrochemical activity as a function of increasing biofilm size, with the cells cultured in the dark giving the lowest current response (Figure S13). The background CV current of the CdrAB strain cultured in the dark on planar ITO was more significant than the background conduction current of the same condition on IDA. This is likely because the cells of nonpatterned biofilms have a higher cytochrome concentration and all the cells on the planar ITO can contribute to the current generation, while the discontinuous dark condition biofilms poorly bridged the IDA source and drain electrodes, resulting in lower conduction current.

Defined Pattern Geometry Was Used to Calculate Biofilm Conductivity. Using the defined biofilm shape from light-patterning, along with confocal microscopy biofilm thickness measurements and the conduction current measured via electrochemical gating, we calculated living CdrAB biofilm conductivity. Unlike conductance, which scales with size of a conductive channel, conductivity is a fundamental material property that is independent of the size of a conductive material. To calculate conductivity using electrochemical gating, the conduction channel bridging the source and drain of an interdigitated electrode must be of uniform length, width, and thickness over the electrode surface.[49] Light-patterning

https://doi.org/10.1021/acssynbio.2c00024
ACS Synth. Biol. XXXX, XXX, XXX−XXX

allowed us to investigate the size-independence of conductivity in biofilms using IDAs with a single fixed geometry. The biofilm thickness on the ITO IDAs of the three patterns sizes was obtained using confocal microscopy (Figure S14), which showed that an approximately 10 μm thick biofilm uniformly formed in the patterned regions for all three sizes, with a thinner (~2 μm thick), sparse layer of cells present in the nonilluminated regions (Figure 4D and 4E). Using the dimensions and conduction current from the three pattern sizes, living CdrAB biofilm conductivity was calculated (see Supplementary Methods) for each pattern and was found to be independent of pattern size and on the order of 4.5 nS/cm. For the small and medium patterned biofilms, only a portion of the interdigitated area was covered with the pattern, while the remaining electrode area was covered with a thinner, patchy cell layer. While it may seem that these conditions created biofilm conduction channels of nonuniform thickness, the similarity in conductivity for all three pattern sizes shows that the off-pattern cell layer did not contribute much to the measured conduction current. It is not possible to calculate a conductivity for the dark condition as it resulted in a patchy layer of cells on the electrode surface (Figure S12) rather than a contiguous conduction channel of uniform length, width, and thickness.

DISCUSSION

We developed a strategy for patterning electroactive bacterial biofilms through the expression of CdrAB aggregation proteins under the control of the blue light-induced pDawn genetic circuit. In this work, several different aggregation proteins were tested with the pDawn genetic circuit since it was not clear which aggregation proteins could mediate adhesion of *S. oneidensis* cells. Of the aggregation proteins tested, only CdrAB encouraged cell−cell adhesion of *S. oneidensis*. Previous studies have shown that CdrA is transported by CdrB to the cell surface and plays a common role as a biofilm matrix cross-linker with different extracellular exopolysaccharides (EPS) to promote aggregation of *P. aeruginosa* cells.[35,50] Due to the close genetic relationship between *Pseudomonas* and *Shewanella*, CdrA may also interact with the EPS of *S. oneidensis* and enable cell aggregation. Although CdrAB expression enabled spatial control over biofilm formation, the cytochrome expression of *Shewanella* was decreased. This resulted in slightly lower EET activity, an issue that warrants further attention. It is not clear why Ag43 and AggA cannot promote cell aggregation despite their expression and association with the outer membrane (Figure S1A). Ag43 is a self-recognizing autotransporter which can promote *E. coli* cell aggregation through self-interaction.[51] But there may be some additional, necessary interactions between Ag43 and EPS or other outer membrane components besides self-interaction of Ag43 to mediate cell aggregation of *Shewanella*. AggA has been reported to be important for cell adhesion and biofilm formation of *Shewanella*, which is the outer-membrane component of the type I secretion system. Perhaps another biofilm-promoting factor BpfA, which is speculated to be secreted to the cell surface through AggA involved type I secretion system, would need to be co-overexpressed and may point to a more supportive role for AggA in cell aggregation.[52,53]

Bacterial biofilm patterning using optogenetic tools has been achieved with several approaches on different substrates without surface pretreatment at a high spatial resolution.[31,32] However, these patterned biofilms have not been naturally electrochemically active. While studies have been done to impart conductivity on *E. coli* patterned biofilms through interfacing self-assembly curli fibers with gold nanoparticles,[54,55] such approaches require modifications of patterned biofilms with conductive nanoparticles. Our patterning strategy allows us to pattern naturally electroactive *S. oneidensis* biofilms without significantly hindering the electrochemical capabilities of the strain.

Prior efforts to direct electroactive biofilm formation on surfaces have focused solely on engineering cell−electrode attachment, rather than patterning, through synthetic biology and materials engineering strategies. These works were based on either (I) enhancing biofilm formation by expressing adhesive appendages on cell surfaces[56,57] and increasing *c*-di-GMP levels[58,59] or (II) placing complementary chemical or DNA-based structures on substrates and cell surfaces to bond cells to electrodes.[60−64] Additionally, a recent study developed a novel conductive polymer coating that enabled the selective deposition of *Shewanella* cells only on a desired region of an electrode surface.[65] Compared with these previous works, our strategy does not require electrode pretreatment for electroactive biofilm patterning and can generate robust biofilms with defined dimensions. As demonstrated in this work, this technique can enable tunable biofilm conduction and electrochemical activity by controlling the amount and location of electroactive cells on unmodified transparent working electrodes.

Additionally, we used the defined geometry of our light-patterned biofilms to, for the first time, quantitatively extract the intrinsic conductivity (~4.5 nS/cm) of living *Shewanella* biofilms. This was not possible previously as *Shewanella* typically makes patchy monolayers on electrode surfaces rather than forming uniform biofilms with defined dimensions, which are required for calculating conductivity.[16] While conductivity was calculated in this work using biofilm geometry that was defined by light-patterning, the underlying IDA electrode geometry could have also been used to define the conductive channel for a uniform, thicker biofilm by constitutively expressing the cell surface adhesins and covering the entire electrode surface. With our newly determined *Shewanella* biofilm conductivity, it is now possible to compare this experimental measurement to recent kinetic Monte Carlo simulations of a newly proposed collision-exchange electron transport mechanism.[66] In that work, micrometer-scale conduction in *S. oneidensis* was proposed to arise from the lateral diffusion of cytochromes, leading to collisions and interprotein electron exchange along cell membranes. Utilizing experimentally determined outer membrane diffusion coefficients and electron hopping rates of *S. oneidensis* cytochromes, simulated conductivity was found to be on the order of 7 nS/cm, in excellent agreement with the conductivity value found in this work. Combining biofilm patterning with known biofilm conductivity can enable designer electrochemical activity and conduction in microbe-based bioelectronics as conductivity allows electron transport to be predicted for a given pattern size.

Although light-induced expression of CdrAB enabled the formation of dense biofilms in blue light-exposed regions of electrode surfaces, cells still attached to unexposed areas of the electrode and produced measurable currents. Future work and applications may benefit from improvements of the current-pattern resolution for defined biofilm dimensions by reducing

https://doi.org/10.1021/acssynbio.2c00024
ACS Synth. Biol. XXXX, XXX, XXX−XXX

attachment of cells in unexposed regions. This may also enable size-dependent current generation of anaerobically patterned biofilms, which are likely to be more conductive than aerobically grown biofilms due to their enhanced cytochrome expression. We have tried to remove the cells in the unexposed regions with orbital shaking to increase shear forces during the washing steps, but there remained cells in the unexposed regions. In future work, synthetic biology strategies could be developed to remove or kill nonspecifically surface-attached cells. Using a *Shewanella* strain deficient in native biofilm formation capabilities, such as a prophage-deficient strain,[67,68] may also be a good approach for eliminating cell presence in the unexposed regions.

Our work provides an avenue for better understanding the relationship between electrochemical activity and electroactive biofilm geometry. Our work also opens the possibility for similar methods to be used to pattern electroactive biofilms of other exoelectrogens. Some approaches have been developed to enhance the EET of native electroactive biofilms by combining them with conductive nanoparticles.[69,70] Thus, patterned biofilms could act as a scaffold for directed conductive nanoparticle biosynthesis or for nanoparticle-biofilm doping to further increase the EET capabilities of patterned biofilms for other applications. In short, we have developed a facile technique to direct the deposition of living conductive biofilms in relation to solid-state electrodes, and we anticipate that this approach will enable further innovations for both studying and harnessing bioelectronics, akin to the role that traditional photolithography played in the development of solid-state electronics.

METHODS

Bacterial Strains, Plasmids, and Growth Conditions. *Escherichia coli* DH5α was used for plasmid construction. *Pseudomonas aeruginosa* PAO1 was used as the source for *cdrAB* genes amplification. *Shewanella oneidensis* MR-1 was used as the host strain.

Plasmid pDawn-Ag43, which contains a blue-light-sensor system and expresses an *E. coli* aggregation protein Ag43, was obtained from *Addgene*.[31] Plasmids pDawn-mCherry, pDawn-AggA, and pDawn-CdrAB were generated through replacing gene *ag43* with *mCherry*, *aggA*, and *cdrAB*, respectively (Figure 1A). Then the above four plasmids were transformed independently into *S. oneidensis* MR-1 via electroporation to generate the corresponding strains. All plasmids, strains, and primers used in this study are listed in Table S1.

Fluorescence Measurement of mCherry and Cell Clumping Assay. Overnight cultures (1%, v/v) of mCherry strain were transferred into 5 mL fresh LB broth and grown to late log phase ($OD_{600\ nm}$ about 1−1.5) under the dark condition to prevent undesired photoactivation. Then, the cultures (1%, v/v) were seeded into 5 mL of LB broth and incubated at 30 °C either under the blue light or dark condition while shaking at 200 rpm. Blue light was provided by attaching LED strip lights to the wall inside the shaker. Cultures were collected after overnight incubation (16 h) to measure the fluorescence of mCherry and the cell optical density ($OD_{600\ nm}$). Quantitative mCherry measurements were performed via a plate reader (Infinite 200 PRO, Tecan) at an excitation wavelength of 590 nm and an emission wavelength of 650 nm. The $OD_{600\ nm}$ was determined using a spectrophotometer (Spectronic 200, Thermo Scientific). Relative fluorescence intensity was calculated by normalization against per $OD_{600\ nm}$ of whole cells. Fluorescence of mCherry was imaged via fluorescent microscope equipped with 100× oil immersion objective lens (Eclipse Ti, Nikon).

For the cell clumping assay, late log phase cultures ($OD_{600\ nm}$ about 1−1.5) of *Shewanella* strains containing different aggregation proteins were transferred into (1%, v/v) 5 mL fresh minimal medium and incubated overnight (16 h) at 30 °C under either blue light or dark conditions while shaking at 200 rpm. Then, the cultures were left to rest for 30 min. The upper region cultures of the tube were collected to measure the OD_{top}. Then, the cultures were rigorously vortexed for 10 s and the OD_{total} was determined. The aggregation index was defined as $\frac{OD_{total(light)} / OD_{total(dark)}}{OD_{top(light)} / OD_{top(dark)}}$.

Biofilm Formation Assay and Patterning on Plastic and Glass. The late log phase LB cultures ($OD_{600\ nm}$ about 1−1.5) were diluted into fresh minimal medium to an $OD_{600\ nm}$ of about 0.01. 100 μL of the dilution was added to each well in a 96-well plate for biofilm assays.[44] One mL and 3 mL of the dilution were added to each well of a 12-well plate and to the glass bottom dish for biofilm patterning, respectively. The vessels containing the cultures were taped to the ceiling of a 30 °C incubator. A portable smart projector (A5 Pro, Wowoto) was secured below the vessels in the incubator and pointed up at the bottom surface of the vessels (Figure 2A). 440 nm blue light patterns created in Microsoft PowerPoint were projected onto the underside of the culture vessels.

After the overnight culturing of cells for different times and under different intensities of blue-light illumination, the medium was subsequently discarded. The patterned biofilms were gently washed three times with PBS. Then biofilms formed on the wells and dishes were stained with 0.1% crystal violet for 10 min, rinsed three times with PBS, and dried at room temperature for imaging. Before crystal violet staining, the light-induced biofilm patterned area and unexposed region in the same glass bottom dish were observed via light microscopy. Finally, 30% acetic acid was added to dissolve the absorbed crystal violet for 10 min, and A550 nm quantification of the solution was determined by plate reader.

An adjustable neutral density filter (KF01.063, K&F Concept) was used for tuning the illumination intensity by placing it at the aperture of the projector. An optical power meter (PM100USB, Thorlabs) was used for measuring the illumination intensity of the projected patterns.

For patterning on the surface of indium tin oxide (ITO) coated glass coverslips and custom ITO IDAs ahead of electrochemical measurements, 1 mL of diluted cells were added to the bioreactor, which was made by attaching a 20 mm diameter and 2.5 cm tall glass tube on an electrode. During the incubation, the glass tubes were sealed with a microporous membrane filter (AirOtop Seals). After 16 h of patterning, medium was discarded, and the patterned biofilms were washed five times, for 10 min each time, with PBS or nonturnover minimal medium in a shaker at 220 rpm to reduce the nonspecific patterned cells.

Resting Cell Ferrozine Assay. Resting cell ferrozine assay was modified on the basis of a previous study.[22] Cells from late log phase LB cultures were diluted into 5 mL fresh minimal medium to an $OD_{600\ nm}$ of about 0.01. Then, cells were incubated for 16 h at 30 °C under either blue light or dark conditions while shaking at 200 rpm. Cells were collected by centrifuging at 4200 rpm, 4 °C for 15 min and then washed

https://doi.org/10.1021/acssynbio.2c00024
ACS Synth. Biol. XXXX, XXX, XXX−XXX

with fresh minimal medium once. After that, cells were inoculated into sealed serum bottles containing 25 mL anaerobic minimal medium to an $OD_{600\ nm}$ of about 0.1. Two mM ferric citrate was added into the anaerobic minimal medium as the electron acceptor. The samples were incubated at 30 °C under dark conditions without shaking. Every 2 h, 10 μL of each sample was added immediately to 90 μL 1 M HCl in a 96-well plate followed by 100 μL 0.01% ferrozine. Then, after mixing the samples well and letting them sit for 10 min, the absorbances of the samples at 562 nm was determined with a plate reader. A standard curve of freshly made ferrous sulfate was used to determine the Fe^{2+} concentrations.

Transparent-Bottom Bioreactor Construction. To observe the surface coverage and thickness of patterned biofilms on bioreactor working electrodes (WEs) in situ, transparent-bottom bioreactors were constructed. Planar, 22 mm by 40 mm commercial indium tin oxide (ITO) coated glass coverslips (Prod no. 06494-AB, Structure Probe, Inc.) or custom ITO IDAs (designed in house and fabricated via foundry service) were used as the bioreactor base. Before use, the commercial ITO glass coverslips and the custom IDAs were rinsed with acetone, isopropanol, and then with DI water, and then dried with N_2. Thin copper wires (Prod no. 1227, TCS 20' 32 gauge wire) were electrically connected to the WEs with silver paint (Prod no. 16035, TED PELLA, Inc.). To mechanically strengthen the wire-electrode connections, they were covered with epoxy (Gorilla Glue Co.). Functioning as the body of the bioreactors, glass tubes (2.5 cm tall with a 19 mm and 22 mm inner and outer diameter, respectively) were adhered overtop of the WEs with siliconized sealant (DAP Kwik Seal Ultra Premium Siliconized Sealant) (Figure 3B). Custom, PEEK plastic lids were used with the transparent-bottom reactors along with custom Pt wire counter electrodes (CEs) and 1 M KCl Ag/AgCl reference electrodes (REs) (CHI111P, CH Instruments, Inc.) (Figure 3B). All potentials reported in this manuscript are vs 1 M KCl Ag/AgCl.

Measurements of Electrochemical Activity and Biofilm Conduction. All electrochemical measurements were performed in an anaerobic chamber (Bactron 300, Sheldon Manufacturing, Inc.) with a 95:5 (N_2/H_2) atmosphere. Sterile medium (blank) electrochemical measurements were performed before reactors were used in biofilm patterning. For the commercial ITO reactors, minimal media was used for the blank measurements, while nonturnover (NT) minimal media was used for the interdigitated array (IDA) blank measurements. During the patterning steps, the CEs and REs were removed from the reactors and the reactors were simply used as a culturing vessel. For the commercial ITO reactors, blank and biofilm cyclic voltammetry (CV) measurements were performed from −500 mV to either 200 or 300 mV at 1 mV/s using a four channel Squidstat (Admiral Instruments). To perform the electrochemical gating done with the IDA reactors, two Gamry Reference 600 potentiostats connected with a synchronization cable and operating in bipotentiostat mode were used. Blank gating scans were also performed before patterning. For the blank and biofilm gating measurements, the IDA working electrodes (WEs) were scanned at rate of 1 mV/s from −500 to 300 mV but with a fixed gating offset V_{SD} = 20 mV, where $V_{SD} = E_D - E_S$ and where E_D and E_S are the potentials at each of the IDA WEs. To determine I_{cond}, we first assumed that equal and opposite sign I_{cond} plus background currents of the same sign were measured at each IDA WE. Then, I_{cond} could be calculated by subtracting the drain and source currents and dividing by two, $(I_D - I_S)/2$. Three cycles were performed for both the CV and gating scans and only data from the third cycle is presented in this manuscript. Ahead of anaerobic patterning, the reactors were sealed with sterile rubber stoppers before being removed from the anaerobic chamber. After aerobic patterning, inside the anaerobic chamber, the reactor media was exchanged for anaerobic media before all electrochemical measurements. Prior to the size-dependent CV and gating scans, chronoamperometry (CA) was performed on the reactors for 1 to 6 h with the WEs held at 200 mV.

Statistical Analysis. All statistical analyses were performed by the Prism software (version 9.0; GraphPad) using one-way ANOVA with Dunnett's multiple comparisons test or two-tailed unpaired *t* test. All data are presented as the mean ± SD. *P* values in all graphs were generated with tests as indicated in figure legends and are represented as follows: $*p < 0.05$, $**p < 0.01$, $***p < 0.001$, $****p < 0.0001$, and ns (not significant) $p > 0.05$.

■ ASSOCIATED CONTENT

Supporting Information

The Supporting Information is available free of charge at https://pubs.acs.org/doi/10.1021/acssynbio.2c00024.

Supplementary Methods: Growth conditions; Aggregation proteins extraction; TMBZ heme stain SDS-PAGE protein gel; Microfabrication of custom IDA electrodes; Additional technical notes about the electrochemical gating measurements; Microscopy observations of patterned biofilms on electrodes; Biofilm thickness analysis; Line edge roughness analysis; Calculation of patterned biofilm conductivity; Figures S1−S15: SDS-PAGE gel images of aggregation proteins; Optimization of the biofilm formation under different light intensities and illumination time; Biofilm patterning on plastic substrates; Biofilm patterning on glass substrates; Optimization of biofilm patterning using glass tubes; TMBZ heme stain SDS-PAGE protein gel; Biofilm patterning on the ITO coated glass electrodes; Representative CV curves for anaerobically patterned CdrAB biofilms; Line edge roughness for the patterning on custom transparent ITO IDA electrodes; Representative source and drain CV curves for patterned CdrAB biofilms of different sizes on custom transparent ITO IDA electrodes; Schematic of how we change the biofilm sizes on custom transparent ITO IDA electrodes; Confocal microscope images for the CdrAB dark condition on ITO IDA electrode; Triplicate CV curves for patterned biofilms of CdrAB with different sizes on planar ITO electrodes; Examples for biofilm thickness measurements; Peak I_{cond} vs varying gating offsets for the medium-sized CdrAB pattern; Table S1: Strains, plasmids, and primers used in this study (PDF)

■ AUTHOR INFORMATION

Corresponding Author

James Q. Boedicker − *Department of Physics and Astronomy and Department of Biological Sciences, University of Southern California, Los Angeles, California 90089, United States*; Email: boedicke@usc.edu

https://doi.org/10.1021/acssynbio.2c00024
ACS Synth. Biol. XXXX, XXX, XXX−XXX

Authors

Fengjie Zhao − *Department of Physics and Astronomy, University of Southern California, Los Angeles, California 90089, United States;* orcid.org/0000-0003-2279-5062

Marko S. Chavez − *Department of Physics and Astronomy, University of Southern California, Los Angeles, California 90089, United States*

Kyle L. Naughton − *Department of Physics and Astronomy, University of Southern California, Los Angeles, California 90089, United States;* orcid.org/0000-0002-1079-0240

Christina M. Niman − *Department of Physics and Astronomy, University of Southern California, Los Angeles, California 90089, United States*

Joshua T. Atkinson − *Department of Physics and Astronomy, University of Southern California, Los Angeles, California 90089, United States;* orcid.org/0000-0001-9293-4123

Jeffrey A. Gralnick − *BioTechnology Institute and Department of Plant and Microbial Biology, University of Minnesota−Twin Cities, St. Paul, Minnesota 55108, United States;* orcid.org/0000-0001-9250-7770

Mohamed Y. El-Naggar − *Department of Physics and Astronomy, Department of Biological Sciences, and Department of Chemistry, University of Southern California, Los Angeles, California 90089, United States;* orcid.org/0000-0001-5599-6309

Complete contact information is available at: https://pubs.acs.org/10.1021/acssynbio.2c00024

Author Contributions

#F.Z. and M.S.C. contributed equally to the work. F.Z., M.S.C., J.A.G., M.Y.E.-N., and J.Q.B. designed research; F.Z., M.S.C., K.L.N., and C.M.N. performed research; F.Z., M.S.C., K.L.N., and J.T.A. analyzed data; and F.Z., M.S.C., M.Y.E.-N., and J.Q.B. wrote the paper. All authors edited the manuscript.

Notes

The authors declare no competing financial interest.

All relevant data supporting the key findings of this study are available within the article and Supporting Information. Plasmids and strains generated for this study will be shared upon request to the corresponding author.

■ ACKNOWLEDGMENTS

The electrodes used in this work were fabricated at the San Diego Nanotechnology Infrastructure (SDNI) of UCSD, a member of the National Nanotechnology Coordinated Infrastructure, which is supported by the National Science Foundation (Grant ECCS-2025752). We thank Karla Abuyen for the help of modifying illustrations and Cesar Rodriguez for preliminary work on this project. This study was supported by the US Office of Naval Research Multidisciplinary University Research Initiative Grant No. N00014-18-1-2632. J.T.A. was supported by the NSF Postdoctoral Research Fellowships in Biology Program under Grant No. 2010604.

■ REFERENCES

(1) Myers, C. R.; Nealson, K. H. Bacterial manganese reduction and growth with manganese oxide as the sole electron acceptor. *Science* **1988**, *240*, 1319−1321.

(2) Lovley, D. R.; Stolz, J. F.; Nord, G. L.; Phillips, E. J. P. Anaerobic production of magnetite by a dissimilatory iron-reducing microorganism. *Nature* **1987**, *330*, 252−254.

(3) Shi, L.; Dong, H.; Reguera, G.; Beyenal, H.; Lu, A.; Liu, J.; Yu, H. Q.; Fredrickson, J. K. Extracellular electron transfer mechanisms between microorganisms and minerals. *Nat. Rev. Microbiol.* **2016**, *14*, 651−662.

(4) McMillan, D. G. G.; Marritt, S. J.; Butt, J. N.; Jeuken, L. J. C. Menaquinone-7 is specific cofactor in tetraheme quinol dehydrogenase CymA. *J. Biol. Chem.* **2012**, *287*, 14215−14225.

(5) Edwards, M. J.; White, G. F.; Lockwood, C. W.; Lawes, M. C.; Martel, A.; Harris, G.; Scott, D. J.; Richardson, D. J.; Butt, J. N.; Clarke, T. A. Structural modeling of an outer membrane electron conduit from a metal-reducing bacterium suggests electron transfer via periplasmic redox partners. *J. Biol. Chem.* **2018**, *293*, 8103−8112.

(6) Fonseca, B. M.; Paquete, C. M.; Neto, S. E.; Pacheco, I.; Soares, C. M.; Louro, R. O. Mind the gap: Cytochrome interactions reveal electron pathways across the periplasm of *Shewanella oneidensis* MR-1. *Biochem. J.* **2013**, *449*, 101−108.

(7) Hartshorne, R. S.; Reardon, C. M.; Ross, D.; Nuester, J.; Clarke, T. A.; Gates, A. J.; Mills, P. C.; Fredrickson, J. K.; Zachara, J. M.; Shi, L.; Beliaev, A. S.; Marshall, M. J.; Tien, M.; Brantley, S.; Butt, J. N.; Richardson, D. J. Characterization of an electron conduit between bacteria and the extracellular environment. *Proc. Natl. Acad. Sci. U. S. A.* **2009**, *106*, 22169−22174.

(8) White, G. F.; Shi, Z.; Shi, L.; Wang, Z.; Dohnalkova, A. C.; Marshall, M. J.; Fredrickson, J. K.; Zachara, J. M.; Butt, J. N.; Richardson, D. J.; Clarke, T. A. Rapid electron exchange between surface-exposed bacterial cytochromes and Fe(III) minerals. *Proc. Natl. Acad. Sci. U. S. A.* **2013**, *110*, 6346−6351.

(9) Edwards, M. J.; White, G. F.; Butt, J. N.; Richardson, D. J.; Clarke, T. A. The crystal structure of a biological insulated transmembrane molecular wire. *Cell* **2020**, *181*, 665−673.

(10) Marsili, E.; Baron, D. B.; Shikhare, I. D.; Coursolle, D.; Gralnick, J. A.; Bond, D. R. *Shewanella* secretes flavins that mediate extracellular electron transfer. *Proc. Natl. Acad. Sci. U. S. A.* **2008**, *105*, 3968−3973.

(11) Coursolle, D.; Baron, D. B.; Bond, D. R.; Gralnick, J. A. The Mtr respiratory pathway is essential for reducing flavins and electrodes in *Shewanella oneidensis*. *J. Bacteriol.* **2010**, *192*, 467−474.

(12) Pirbadian, S.; Barchinger, S. E.; Leung, K. M.; Byun, H. S.; Jangir, Y.; Bouhenni, R. A.; Reed, S. B.; Romine, M. F.; Saffarini, D. A.; Shi, L.; Gorby, Y. A.; Golbeck, J. H.; El-Naggar, M. Y. *Shewanella oneidensis* MR-1 nanowires are outer membrane and periplasmic extensions of the extracellular electron transport components. *Proc. Natl. Acad. Sci. U. S. A.* **2014**, *111*, 12883−12888.

(13) Xu, S.; Jangir, Y.; El-Naggar, M. Y. Disentangling the roles of free and cytochrome-bound flavins in extracellular electron transport from *Shewanella oneidensis* MR-1. *Electrochim. Acta* **2016**, *198*, 49−55.

(14) Zacharoff, L. A.; El-Naggar, M. Y. Redox conduction in biofilms: From respiration to living electronics. *Curr. Opin. Electrochem.* **2017**, *4*, 182−189.

(15) Snider, R. M.; Strycharz-Glaven, S. M.; Tsoi, S. D.; Erickson, J. S.; Tender, L. M. Long-range electron transport in *Geobacter sulfurreducens* biofilms is redox gradient-driven. *Proc. Natl. Acad. Sci. U. S. A.* **2012**, *109*, 15467−15472.

(16) Xu, S.; Barrozo, A.; Tender, L. M.; Krylov, A. I.; El-Naggar, M. Y. Multiheme cytochrome mediated redox conduction through *Shewanella oneidensis* MR-1 cells. *J. Am. Chem. Soc.* **2018**, *140*, 10085−10089.

(17) Yates, M. D.; Golden, J. P.; Roy, J.; Strycharz-Glaven, S. M.; Tsoi, S.; Erickson, J. S.; El-Naggar, M. Y.; Barton, S. C.; Tender, L. M. Thermally activated long range electron transport in living biofilms. *Phys. Chem. Chem. Phys.* **2015**, *17*, 32564−32570.

(18) Logan, B. E.; Rabaey, K. Conversion of wastes into bioelectricity and chemicals by using microbial electrochemical technologies. *Science* **2012**, *337*, 686−690.

(19) Tanzil, A. H.; Sultana, S. T.; Saunders, S. R.; Dohnalkova, A. C.; Shi, L.; Davenport, E.; Ha, P.; Beyenal, H. Production of gold nanoparticles by electrode-respiring *Geobacter sulfurreducens* biofilms. *Enzyme Microb. Technol.* **2016**, *95*, 69−75.

(20) Zhang, Y.; Hsu, L. H. H.; Jiang, X. Living electronics. *Nano Res.* **2020**, *13*, 1205−1213.

(21) Yim, S. S.; McBee, R. M.; Song, A. M.; Huang, Y.; Sheth, R. U.; Wang, H. H. Robust direct digital-to-biological data storage in living cells. *Nat. Chem. Biol.* **2021**, *17*, 246−253.
(22) West, E. A.; Jain, A.; Gralnick, J. A. Engineering a native inducible expression system in *Shewanella oneidensis* to control extracellular electron transfer. *ACS Synth. Biol.* **2017**, *6*, 1627−1634.
(23) Cao, Y.; Li, X.; Li, F.; Song, H. CRISPRi-sRNA: Transcriptional-translational regulation of extracellular electron transfer in *Shewanella oneidensis*. *ACS Synth. Biol.* **2017**, *6*, 1679−1690.
(24) Li, F. H.; Tang, Q.; Fan, Y. Y.; Li, Y.; Li, J.; Wu, J. H.; Luo, C. F.; Sun, H.; Li, W. W.; Yu, H. Q. Developing a population-state decision system for intelligently reprogramming extracellular electron transfer in *Shewanella oneidensis*. *Proc. Natl. Acad. Sci. U. S. A.* **2020**, *117*, 23001−23010.
(25) Jensen, H. M.; Albers, A. E.; Malley, K. R.; Londer, Y. Y.; Cohen, B. E.; Helms, B. A.; Weigele, P.; Groves, J. T.; Ajo-Franklin, C. M. Engineering of a synthetic electron conduit in living cells. *Proc. Natl. Acad. Sci. U. S. A.* **2010**, *107*, 19213−19218.
(26) Jensen, H. M.; TerAvest, M. A.; Kokish, M. G.; Ajo-Franklin, C. M. CymA and exogenous flavins improve extracellular electron transfer and couple it to cell growth in Mtr-expressing *Escherichia coli*. *ACS Synth. Biol.* **2016**, *5*, 679−688.
(27) Su, L.; Fukushima, T.; Prior, A.; Baruch, M.; Zajdel, T. J.; Ajo-Franklin, C. M. Modifying cytochrome c maturation can increase the bioelectronic performance of engineered *Escherichia coli*. *ACS Synth. Biol.* **2020**, *9*, 115−124.
(28) Levskaya, A.; Chevalier, A. A.; Tabor, J. J.; Simpson, Z. B.; Lavery, L. A.; Levy, M.; Davidson, E. A.; Scouras, A.; Ellington, A. D.; Marcotte, E. M.; Voigt, C. A. Engineering *Escherichia coli* to see ligh. *Nature* **2005**, *438*, 441−442.
(29) Ohlendorf, R.; Vidavski, R. R.; Eldar, A.; Moffat, K.; Möglich, A. From dusk till dawn: One-plasmid systems for light-regulated gene expression. *J. Mol. Biol.* **2012**, *416*, 534−542.
(30) Tabor, J. J.; Levskaya, A.; Voigt, C. A. Multichromatic control of gene expression in *Escherichia coli*. *J. Mol. Biol.* **2011**, *405*, 315−324.
(31) Jin, X.; Riedel-Kruse, I. H. Biofilm Lithography enables high-resolution cell patterning via optogenetic adhesin expression. *Proc. Natl. Acad. Sci. U. S. A.* **2018**, *115*, 3698−3703.
(32) Moser, F.; Tham, E.; González, L. M.; Lu, T. K.; Voigt, C. A. Light-controlled, high-resolution patterning of living engineered bacteria onto textiles, ceramics, and plastic. *Adv. Funct. Mater.* **2019**, *29*, 1−11.
(33) Huang, Y.; Xia, A.; Yang, G.; Jin, F. Bioprinting living biofilms through optogenetic manipulation. *ACS Synth. Biol.* **2018**, *7*, 1195−1200.
(34) Chen, F.; Wegner, S. V. Blue-light-switchable bacterial cell-cell adhesions enable the control of multicellular bacterial communities. *ACS Synth. Biol.* **2020**, *9*, 1169−1180.
(35) Borlee, B. R.; Goldman, A. D.; Murakami, K.; Samudrala, R.; Wozniak, D. J.; Parsek, M. R. *Pseudomonas aeruginosa* uses a cyclic-di-GMP-regulated adhesin to reinforce the biofilm extracellular matrix. *Mol. Microbiol.* **2010**, *75*, 827−842.
(36) Reichhardt, C.; Wong, C.; Passos da Silva, D.; Wozniak, D. J.; Parsek, M. R. CdrA interactions within the *Pseudomonas aeruginosa* biofilm matrix safeguard it from proteolysis and promote cellular packing. *mBio* **2018**, *9*, 1−12.
(37) Pu, L.; Yang, S.; Xia, A.; Jin, F. Optogenetics manipulation enables prevention of biofilm formation of engineered *Pseudomonas aeruginosa* on surfaces. *ACS Synth. Biol.* **2018**, *7*, 200−208.
(38) Henderson, I. R.; Meehan, M.; Owen, P. Antigen 43, a phase-variable bipartate outer membrane protein, determines colony morphology and autoaggregation in *Escherichia coli* K-12. *FEMS Microbiol. Lett.* **1997**, *149*, 115−120.
(39) Danese, P. N.; Pratt, L. A.; Dove, S. L.; Kolter, R. The outer membrane protein, Antigen 43, mediates cell-to-cell interactions within *Escherichia coli* biofilms. *Mol. Microbiol.* **2000**, *37*, 424−432.
(40) De Vriendt, K.; Theunissen, S.; Carpentier, W.; De Smet, L.; Devreese, B.; Van Beeumen, J. Proteomics of *Shewanella oneidensis* MR-1 biofilm reveals differentially expressed proteins, including AggA and RibB. *Proteomics* **2005**, *5*, 1308−1316.
(41) De Windt, W.; Gao, H.; Krömer, W.; Van Damme, P.; Dick, J.; Mast, J.; Boon, N.; Zhou, J.; Verstraete, W. AggA is required for aggregation and increased biofilm formation of a hyper-aggregating mutant of *Shewanella oneidensis* MR-1. *Microbiology* **2006**, *152*, 721−729.
(42) Rybtke, M.; Berthelsen, J.; Yang, L.; Høiby, N.; Givskov, M.; Tolker-Nielsen, T. The LapG protein plays a role in *Pseudomonas aeruginosa* biofilm formation by controlling the presence of the CdrA adhesin on the cell surface. *MicrobiologyOpen* **2015**, *4*, 917−930.
(43) Zhou, G.; Yuan, J.; Gao, H. Regulation of biofilm formation by BpfA, BpfD, and BpfG in *Shewanella oneidensis*. *Front. Microbiol.* **2015**, *6*, 790.
(44) O'Toole, G. A. Microtiter dish Biofilm formation assay. *J. Vis. Exp.* **2010**, 10−11.
(45) Kane, A. L.; Bond, D. R.; Gralnick, J. A. Electrochemical analysis of *Shewanella oneidensis* engineered to bind gold electrodes. *ACS Synth. Biol.* **2013**, *2*, 93−101.
(46) Coursolle, D.; Gralnick, J. A. Reconstruction of extracellular respiratory pathways for iron(III) reduction in *Shewanella oneidensis* strain MR-1. *Front. Microbiol.* **2012**, *3*, 1−11.
(47) Marsili, E.; Rollefson, J. B.; Baron, D. B.; Hozalski, R. M.; Bond, D. R. Microbial biofilm voltammetry: direct electrochemical characterization of catalytic electrode-attached biofilms. *Appl. Environ. Microbiol.* **2008**, *74*, 7329−7337.
(48) Yates, M. D.; Strycharz-Glaven, S. M.; Golden, J. P.; Roy, J.; Tsoi, S.; Erickson, J. S.; El-Naggar, M. Y.; Barton, S. C.; Tender, L. M. Measuring conductivity of living *Geobacter sulfurreducens* biofilms. *Nat. Nanotechnol.* **2016**, *11*, 910−913.
(49) Kankare, J.; Kupila, E. L. In-situ conductance measurement during electropolymerization. *J. Electroanal. Chem.* **1992**, *322*, 167−181.
(50) Reichhardt, C.; Jacobs, H. M.; Matwichuk, M.; Wong, C.; Wozniak, D. J.; Parsek, M. R. The versatile *Pseudomonas aeruginosa* biofilm matrix protein CdrA promotes aggregation through different extracellular exopolysaccharide interactions. *J. Bacteriol.* **2020**, *202*, 1−9.
(51) Heras, B.; Totsika, M.; Peters, K. M.; Paxman, J. J.; Gee, C. L.; Jarrott, R. J.; Perugini, M. A.; Whitten, A. E.; Schembri, M. A. The antigen 43 structure reveals a molecular Velcrolike mechanism of autotransporter-mediated bacterial clumping. *Proc. Natl. Acad. Sci. U. S. A.* **2014**, *111*, 457−462.
(52) Theunissen, S.; De Smet, L.; Dansercoer, A.; Motte, B.; Coenye, T.; Van Beeumen, J. J.; Devreese, B.; Savvides, S. N.; Vergauwen, B. The 285 kDa Bap/RTX hybrid cell surface protein (SO4317) of *Shewanella oneidensis* MR-1 is a key mediator of biofilm formation. *Res. Microbiol.* **2010**, *161*, 144−152.
(53) Theunissen, S.; Vergauwen, B.; De Smet, L.; Van Beeumen, J.; Van Gelder, P.; Savvides, S. N. The agglutination protein AggA from *Shewanella oneidensis* MR-1 is a TolC-like protein and forms active channels in vitro. *Biochem. Biophys. Res. Commun.* **2009**, *386*, 380−385.
(54) Chen, A. Y.; Deng, Z.; Billings, A. N.; Seker, U. O. S.; Lu, M. Y.; Citorik, R. J.; Zakeri, B.; Lu, T. K. Synthesis and patterning of tunable multiscale materials with engineered cells. *Nat. Mater.* **2014**, *13*, 515−523.
(55) Wang, X.; Pu, J.; An, B.; Li, Y.; Shang, Y.; Ning, Z.; Liu, Y.; Ba, F.; Zhang, J.; Zhong, C. Programming cells for dynamic assembly of inorganic nano-objects with spatiotemporal control. *Adv. Mater.* **2018**, *30*, 1−10.
(56) Liu, X.; Zhuo, S.; Jing, X.; Yuan, Y.; Rensing, C.; Zhou, S. Flagella act as *Geobacter* biofilm scaffolds to stabilize biofilm and facilitate extracellular electron transfer. *Biosens. Bioelectron.* **2019**, *146*, 111748.
(57) Leang, C.; Malvankar, N. S.; Franks, A. E.; Nevin, K. P.; Lovley, D. R. Engineering *Geobacter sulfurreducens* to produce a highly cohesive conductive matrix with enhanced capacity for current production. *Energy Environ. Sci.* **2013**, *6*, 1901−1908.

https://doi.org/10.1021/acssynbio.2c00024
ACS Synth. Biol. XXXX, XXX, XXX−XXX

(58) Liu, T.; Yu, Y. Y.; Deng, X. P.; Ng, C. K.; Cao, B.; Wang, J. Y.; Rice, S. A.; Kjelleberg, S.; Song, H. Enhanced *Shewanella* biofilm promotes bioelectricity generation. *Biotechnol. Bioeng.* **2015**, *112*, 2051−2059.
(59) Hu, Y.; Wu, Y.; Mukherjee, M.; Cao, B. A near-infrared light responsive *c*-di-GMP module-based AND logic gate in *Shewanella oneidensis*. *Chem. Commun.* **2017**, *53*, 1646−1648.
(60) Catania, C.; Karbelkar, A. A.; Furst, A. L. Engineering the interface between electroactive bacteria and electrodes. *Joule* **2021**, *5*, 743−747.
(61) Furst, A. L.; Smith, M. J.; Lee, M. C.; Francis, M. B. DNA hybridization to interface current-producing cells with electrode surfaces. *ACS Cent. Sci.* **2018**, *4*, 880−884.
(62) Suo, D.; Fang, Z.; Yu, Y. Y.; Yong, Y. C. Synthetic curli enables efficient microbial electrocatalysis with stainless-steel electrode. *AIChE J.* **2020**, *66*, 9−12.
(63) Young, T. D.; Liau, W. T.; Lee, C. K.; Mellody, M.; Wong, G. C. L.; Kasko, A. M.; Weiss, P. S. Selective promotion of adhesion of *Shewanella oneidensis* on mannose-decorated glycopolymer surfaces. *ACS Appl. Mater. Interfaces* **2020**, *12*, 35767−35781.
(64) Lienemann, M.; TerAvest, M. A.; Pitkänen, J. P.; Stuns, I.; Penttilä, M.; Ajo-Franklin, C. M.; Jäntti, J. Towards patterned bioelectronics: facilitated immobilization of exoelectrogenic *Escherichia coli* with heterologous pili. *Microb. Biotechnol.* **2018**, *11*, 1184−1194.
(65) Tseng, C. P.; Liu, F.; Zhang, X.; Huang, P. C.; Campbell, I.; Li, Y.; Atkinson, J. T.; Terlier, T.; Ajo-Franklin, C. M.; Silberg, J. J.; Verduzco, R. Solution-deposited and patternable conductive polymer thin-film electrodes for microbial bioelectronics. *Adv. Mater.* **2022**, *34*, 2109442.
(66) Chong, G. W.; Pirbadian, S.; Zhao, Y.; Zacharoff, L. A.; Pinaud, F.; El-Naggar, M. Y. Single molecule tracking of bacterial cell surface cytochromes reveals dynamics that impact long-distance electron transport. *Proc. Natl. Acad. Sci. U. S. A.* **2022**, *119*, No. e2119964119.
(67) Wang, X.; Kim, Y.; Ma, Q.; Hong, S. H.; Pokusaeva, K.; Sturino, J. M.; Wood, T. K. Cryptic prophages help bacteria cope with adverse environments. *Nat. Commun.* **2010**, *1*, 147.
(68) Wang, X.; Kim, Y.; Wood, T. K. Control and benefits of CP4−57 prophage excision in *Escherichia coli* biofilms. *ISME J.* **2009**, *3*, 1164−1179.
(69) Jiang, X.; Hu, J.; Lieber, A. M.; Jackan, C. S.; Biffinger, J. C.; Fitzgerald, L. A.; Ringeisen, B. R.; Lieber, C. M. Nanoparticle facilitated extracellular electron transfer in microbial fuel cells. *Nano Lett.* **2014**, *14*, 6737−6742.
(70) Yang, C.; Aslan, H.; Zhang, P.; Zhu, S.; Xiao, Y.; Chen, L.; Khan, N.; Boesen, T.; Wang, Y.; Liu, Y.; Wang, L.; Sun, Y.; Feng, Y.; Besenbacher, F.; Zhao, F.; Yu, M. Carbon dots-fed *Shewanella oneidensis* MR-1 for bioelectricity enhancement. *Nat. Commun.* **2020**, *11*, 1379.

https://doi.org/10.1021/acssynbio.2c00024
ACS Synth. Biol. XXXX, XXX, XXX−XXX